Automated tool for 3D planar magnetic temperature modelling: application to EE and E/PLT core-based components

Reda Bakri, Xavier Margueron, Jean Sylvio Ngoua Teu Magambo, Philippe Le Moigne, Nadir Idir

Automated tool for 3D-planar magnetic temperature modelling: Application to EE and E/PLT core-based components

R. Bakri [1], X. Margueron [1*], J. S. Ngoua Teu Magambo [1], P. Le Moigne [1], N. Idir [1]

[1] Univ. Lille, Arts et Metiers ParisTech, Centrale Lille, HEI, EA 2697 - L2EP - Laboratoire d'Electrotechnique et d'Electronique de Puissance, F-59000 Lille, France
[*] xavier.margueron@centralelille.fr

Abstract:
Thermal performance of power converters is a key issue for the power integration. Temperatures inside active and passive devices can be determined using thermal models. Modelling the temperature distribution of high frequency magnetic components is quite complex due to diversity of their geometries and used materials. This paper presents a thermal modelling method based on lumped elements thermal network model, applied to planar magnetic components made of EE and E/PLT cores. The 3D model is automatically generated from the component's geometry. The computation enables to obtain 3D temperature distribution inside windings and core of planar transformers or inductors, in steady state or in transient case. The paper details the proposed modelling method as well as the automated tool including the problem definition and the solving process. The obtained temperature distributions are compared with Finite Element simulation results and measurements on different planar transformers.

1. Introduction

The current trend in power electronics is to increase power density of converters. Then, volume of power converters is critically reduced and efficiency increased [1, 2], mainly linked to the increase of switching frequencies thanks to wide band gap semiconductors (WBGS) like SiC and GaN [3-5].

In these converters, magnetic components (i.e. inductors and transformers) achieve a number of vital functionalities like energy storage, filtering, transferring, etc. However, magnetic devices occupy an important volume and are a limiting part toward power electronic converter integration. Moreover, unlike active SiC and GaN devices, operating beyond frequencies of MHz is quite impossible for these components with current technologies, especially for high power converters.

Planar magnetic components are a solution to support power electronic integration. These components use low profile ferrite cores and planar windings made of printed circuit board (PCB) tracks or copper foils. Planar magnetics present many advantages compared to wounded components [6, 7]: Low profile, good repeatability, better thermal performances and lower losses at high frequencies (HF). However, they can also present disadvantages such as large footprint, limited number of turns and high winding stray capacitances. The latter topic is an important issue, especially for LLC converters [8].

Increasing the switching frequencies of power converters allow to reduce the magnetic device volume from the electrical functionality point of view. On the other side, from the efficiency point of view, it increases losses and, as a consequence, the temperature of the device. Then, the HF benefits are mainly limited by the thermal constraints. Therefore, thermal modelling of magnetic components is a key point at the design stage to insure the thermal integrity of the components during their life cycle.

Overall, the thermal modelling in electrical engineering and especially for magnetic components can be performed using several approaches [9]. Devices can be modelled in a simple way by a unique thermal resistance that links the temperature rise to the amount of power losses. This thermal resistance can be estimated from physical and geometrical properties of the component. More complex models can also be achieved with nodal thermal resistance networks. Such models are based on thermal and electrical circuit's analogy. The accuracy of this method depends on the node number as well as on element choices. Nodal models can require fitting from experimental results. With the development of numerical tools, finite element method (FEM) and computational fluid dynamic (CFD) are widely used for thermal modelling. FEM solves heat equation in solids, with boundary conditions represented by a heat transfer coefficients fixed in the external area of the component [10]. For such models, the main challenge deals with the determination of these heat transfer coefficients. Regarding CFD analysis, heat transfer is solved in solids and fluids taking into account fluid movements. That leads to an accurate modelling of convection but it needs to model the air around the component which leads to a more complex numerical problem in comparison with FEM.

Regarding planar magnetics, the component's temperature rise can be evaluated during the design stage with the equivalent thermal resistance [11-13]. Some expressions of such thermal resistance for planar magnetic cores are given in the literature [14-18]. In [14, 15], the calculation is based on the effective volume of the core. In [16, 17], the thermal resistance is calculated from the external area of the component. These both values are fixed ones and time-independent. In [18], a global thermal resistance depending on ambient temperature and power losses is proposed for E/PLT cores. Other models available in the literature are based on more detailed networks [19-24]. In [19], a simplified 1D model leads to a RC network that is used to estimate the temperature of the component. In [20], the component's mean

temperature is obtained with a detailed thermal resistance network. The mean value is due to winding homogenization and reduced nodes. A semi-analytical 2D transient model, based on Green's functions has been developed in [21, 22]. This model needs top and bottom device temperatures as inputs. In [23], 3D finite element analysis (FEA) have been applied to a planar transformer to calculate its temperature distribution. Investigations on solutions to decrease the temperature of the component are also developed. Usually, models proposed in the literature do not often take into account the 3D thermal aspect of planar magnetics, neither different kind of limit conditions especially when they depend on the component's temperature. In [24], the authors have investigate this problematic in the case of EE and ER planar cores. The model, based on lumped parameter thermal network enable to obtain temperature inside magnetic cores in transient cases. Temperatures inside the windings are not available. Therefore, potential windings' destructive hot spots cannot be considered.

In this paper, a full 3D automated lumped elements thermal model for planar magnetics and its dedicated tool are presented. The thermal model network is automatically generated from the geometrical description of the component (i.e windings and core), material properties and power losses. Conduction, convection and radiation are taken into account in the temperature distribution calculation. The thermal problem can be solved in steady state and transient case.

The proposed tool presents some advantages:

i. No geometrical approximation is needed: detailed windings are represented without any homogenization.

ii. Lumped elements are automatically computed according to the physical topology of the component.

iii. The temperature distribution in windings and magnetic core is accurately represented in 3D.

iv. Four mode of resolutions are selectable (steady state and transient case with or without temperature dependent coefficients).

v. Each type of EE and E/PLT core based planar transformers and inductors can be easily modeled.

vi. No extra experimental fitting effort is needed

vii. The ratio accuracy/computation time is advantageous and suitable for design and optimization process

The paper is organized as follows: Section II introduces basis for modelling and solving of thermal resistance networks. Then, hypothesis for the thermal modelling of planar magnetics are discussed. Section III details the thermal automated tool dedicated to planar magnetics: The discretization of the considered component is presented as well as the derivation of the different elements of the thermal resistance network. In section IV, the model is applied to two study cases and compared to FEM simulation results. Finally, an experimental validation with two planar transformer prototypes is performed and discussed.

2. Modelling basis

The thermal modelling of planar magnetics developed in this paper is based on thermal resistance networks (TRN). In the following paragraphs, equations and solving of such models are described and hypothesis for the planar magnetic thermal modelling are also addressed.

2.1. Equations for thermal resistance network

A general TRN is shown in Fig.1. The node, indexed i, is linked with other nodes, indexed j, by thermal resistances noted R_{ij}. Losses in the node are modelled by a current source q_i. Node i is also linked to the thermal ground by a thermal capacitance C_i representing dynamic effects.

Let's suppose that nodes 1 to m have unknown temperatures that must be calculated. Temperatures of nodes $m+1$ to n are known. These known temperatures could be measured, or computed from models of cooling systems, as it can be temperatures from an isothermal face in the case of ideal cold plate. In fact, such model resolution does not need complementary measurements.

The thermal equilibrium is derived from Kirchhoff laws applied to the node i:

$$\sum_{j=1}^{n} \frac{T_i - T_j}{R_{ij}} - q_i = -C_i \frac{dT_i}{dt} \tag{1}$$

Indexes 1 to m with unknown temperatures are separated from indexes $m+1$ to n with known temperatures (2):

$$\left(\sum_{j=1}^{n} \frac{1}{R_{ij}} \right) T_i - \sum_{j=1}^{m} \frac{1}{R_{ij}} T_j - \sum_{j=m+1}^{n} \frac{1}{R_{ij}} T_j - q_i = -C_i \frac{dT_i}{dt} \tag{2}$$

The use of thermal admittances G_{ij} (2) is preferred to thermal resistances R_{ij}. Indeed, when two nodes are not linked, it means that they are linked with an infinite thermal resistance or a zero thermal admittance.

$$G_{ij} = \frac{1}{R_{ij}} \tag{3}$$

Then, using admittances is more suitable for numerical computations. Eq (2) becomes:

$$\left(\sum_{j=1}^{n} G_{ij} \right) . T_i - \sum_{j=1}^{m} G_{ij} T_j - \sum_{j=m+1}^{n} G_{ij} T_j - q_i = -C_i \frac{dT_i}{dt} \tag{4}$$

Equation (4) can be rewritten under a matrix form for all nodes i, from 1 to m:

$$AT - BU = -C \frac{dT}{dt} \tag{5}$$

Where:

A is the admittance matrix

U is the vector of losses and known temperatures.

T is the unknown temperatures vector to be calculated.

C is the thermal capacitance matrix

Those vectors and matrixes are given by:

$$A = \begin{pmatrix} \sum_{j=1}^{n} G_{1j} & -G_{12} & \cdots & -G_{1m} \\ -G_{12} & \sum_{j=1}^{n} G_{2j} & & -G_{2m} \\ \vdots & \vdots & \ddots & \vdots \\ -G_{1m} & -G_{m2} & \cdots & \sum_{j=1}^{n} G_{mj} \end{pmatrix} \qquad T = \begin{pmatrix} T_1 \\ T_2 \\ \vdots \\ T_m \end{pmatrix} \tag{6}$$

$$B = \begin{pmatrix} 1 & 0 & \cdots & 0 & G_{1(m+1)} & G_{1(m+2)} & \cdots & G_{1n} \\ 0 & 1 & \cdots & 0 & G_{2(m+1)} & G_{2(m+2)} & \cdots & G_{2n} \\ \vdots & \vdots & \ddots & \vdots & \vdots & \vdots & \cdots & \vdots \\ 0 & 0 & \cdots & 1 & G_{m(m+1)} & G_{m(m+2)} & \cdots & G_{mn} \end{pmatrix} \quad U = \begin{pmatrix} q_1 \\ q_2 \\ \vdots \\ q_m \\ T_{m+1} \\ T_{m+2} \\ \vdots \\ T_n \end{pmatrix}$$

$$C = \begin{pmatrix} C_1 & 0 & \cdots & 0 \\ 0 & C_2 & & 0 \\ \vdots & \vdots & \ddots & \vdots \\ 0 & 0 & \cdots & C_m \end{pmatrix}$$

2.2. Thermal problem solving

From formulation (5), two cases have to be distinguished for the solving process: the steady state case and the transient case.

2.2.1. Steady state: In steady state the temperature is constant, then $\frac{dT}{dt} = 0$. Equation (5) can be rewritten as:

$$AT - BU = 0 \tag{7}$$

The temperature vector is extracted from (8). This expression can be calculated with any mathematical software.

$$T = A^{-1}BU \tag{8}$$

2.2.2. Transient case: In transient case, the temperature vector (T) is time dependent. Power losses and imposed temperatures (U vector) can be also time dependent. Iterative methods must be introduced to evaluate temperatures. The derivative term has to be approximated. In our case, an Euler scheme is chosen as an approximation of the derivative term. The equation (5) becomes:

$$AT^{k+1} - BU^k = C\frac{T^k - T^{k+1}}{\Delta t} \tag{9}$$

From relation (9), the temperature vector for the $k+1$ iteration is given by (10). An initial temperature vector T^0 must be defined to solve this equation.

$$T^{k+1} = \left(A + \frac{C}{\Delta t}\right)^{-1}\left[BU^k + \frac{C}{\Delta t}T^k\right] \tag{10}$$

2.3. Modelling Hypotheses

According to its geometrical symmetry, a quarter of a planar magnetic component (Fig.2) is considered for the thermal modelling. Hypotheses must be made to model all heat transfer phenomena:

i. Heat flux is supposed to be independent in the three directions of the Cartesian reference.

ii. Radiation and convection inside the component's window are negligible.

iii. Air inside the core window is represented as a solid material (i.e. no convection).

iv. Losses are supposed to be homogeneous and loss density is constant inside every winding's turn, as well as inside the core.

3. Thermal automated tool for planar magnetics (TATPM)

An automated tool for the 3D-temperature distribution computation of planar magnetics has been developed, based on a thermal resistance lumped element model. The Fig.3 presents the overview of the thermal automated tool for planar magnetics (TATPM).

The flowchart (Fig.3) is divided in three parts. The first one deals with the user actions that inputs data for the modelling. The two others are linked to the solving process. The component geometry and its mesh are automatically generated while the thermal resistances are computed based on geometry, data and boundary conditions. The last part deals with the solving options, including transient and steady state, with constant or dependent temperature boundary conditions.

In the following paragraphs, all the elements of the TATPM are detailed: Geometry description, nodes, thermal resistances, thermal capacitances, losses distribution, as well as boundary conditions and solving process.

3.1. Geometry description

The first input of TATPM is the geometry description of the planar component: core and windings. Other inputs deal with the materials physical properties: thermal conductivities, density and specific heat capacity, as well as losses in the component.

In order to be useful and practical for designers, the geometry description is parametrized and adapted to all EE and E/PLT planar magnetic core sizes [25]. In TATPM, all the elements are described in a matrix format. Magnetic core geometrical parameters are shown in Fig.4. These values can be easily found in manufacturer datasheets.

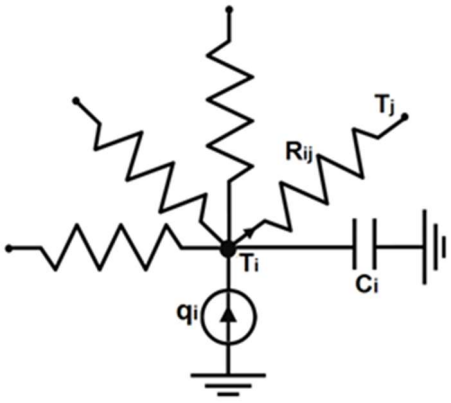

Fig. 1. *Thermal circuit for node i*

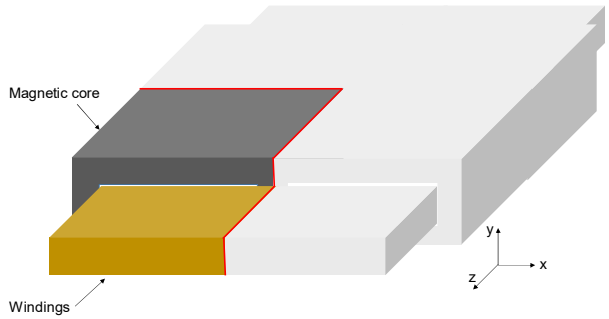

Fig. 2. *Planar magnetic under study*

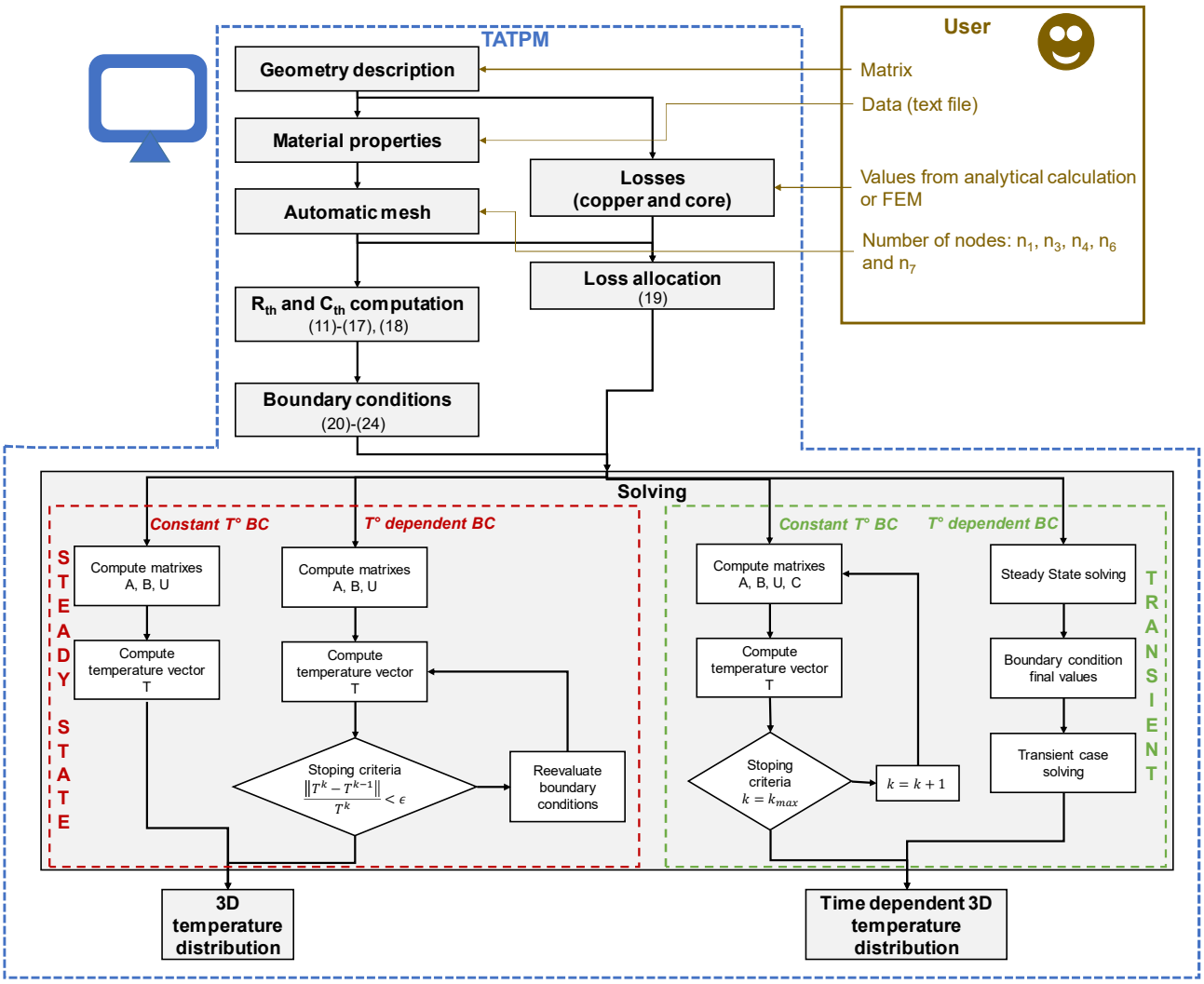

Fig. 3. *Overview of the automated tool (TATPM)*

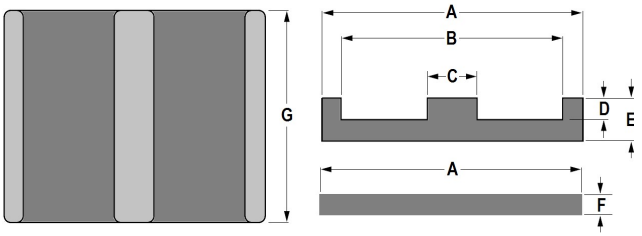

Fig. 4. *Geometric parameters of planar cores (E and PLT shape)*

Regarding windings, copper layers are described with a set of parameters as shown in Fig.5a. Those parameters describe the conductors and insulators sizes as well as their position in the window. Fig.5b shows an example of a geometry automatically generated from parameters described in matrix form. The component's discretization is visible in this example. This discretization based on parallelepiped elements is detailed bellow.

3.2. Component discretization and thermal resistances computation

The component's discretization allows the placement of all the thermal resistances. The computation of their values depends on the size and the positioning of the component's various elements. Then, core and windings are discretised by respecting some constraints. The latter can be of two kinds. Either they are linked to the number of elements on component's parts, or it is fixed (Fig.6).

For the core:

- n_1, n_3, n_4, n_6 and n_7 are fixed by the user.
- n_2 depends on the number of conductors' layers and insulator ones.
- n_5 and n_8 are fixed from the number of turns in the external conductor layers of the winding, in order to make the link between windings and core more easily.

In the conductor's plane, the same number of elements as in the core (n_7) is applied. Other elements are added to each conductor in their part outside the core, from the boundary of the other conductors.

In practice, n_1, n_3, n_4 and n_6 are the same. From our experience regarding the use of TATPM, choosing 3 elements for n_1, n_3, n_4 and n_6, and 4 elements for n_7, leads to accurate results. Increasing the number of elements do not lead to more accuracy. Then, for the case studies presented in this paper, these values are applied. From this discretization, the different thermal resistances are placed as shown in Fig.7. Most of the thermal resistances (R_{tu}, R_{in}, R_{it}, R_{ci}, R_{wc} and R_c) represent thermal conduction phenomenon. Other thermal resistances (R_{ex}) are added to model the convective and radiative thermal exchanges with ambient air.

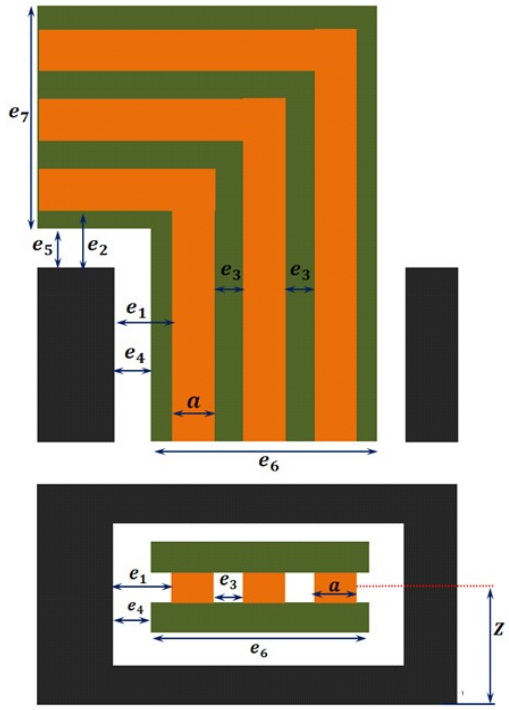

a

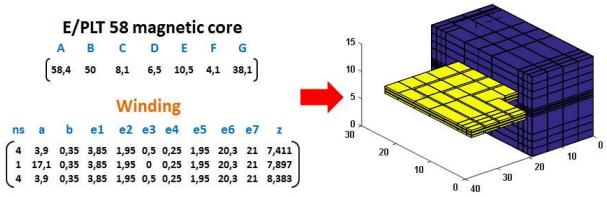

b

Fig. 5. *Geometric parameters of windings*
(a) Top and front view, ***(b)*** Example of generated geometry from matrix description

3.2.1. R_{tu}: This thermal resistance represents conduction phenomena inside the copper layers in the direction of turns. This resistance appears between two adjacent elements of a turn (Fig.8a). Its value is given by the relation (11).

$$R_{tu} = \frac{e_{tu}}{k_{Cu} \cdot S_{tu}} \tag{11}$$

with k_{Cu}, the thermal conductivity of copper.

3.2.2. R_{in}: It represents conduction phenomena inside the insulator. It can be calculated with similar expression (12).

$$R_{in} = \frac{e_{in}}{k_i \cdot S_{in}} \tag{12}$$

with k_i, the thermal conductivity of insulator, e_{in} and S_{in}, length and section of the discretised element.

3.2.3.R_{it}, R_{wc} *and* R_c: These thermal resistances represent conduction phenomena inside inter-turns insulator (R_{it}), between the winding and the core (R_{wc}) and inside the core (R_c). Fig.8b shows geometrical elements and corresponding thermal resistances. Their values are calculated with equations (13), (14), and (15) respectively.

$$R_{it} = \left(\frac{e_{Cu}}{k_{Cu}} + \frac{e_{it}}{k_{it}} \right) \cdot \frac{1}{S_{it}} \tag{13}$$

$$R_{wc} = \left(\frac{e_{Cu}}{k_{Cu}} + \frac{e_g}{k_g} + \frac{e_c}{k_c} \right) \cdot \frac{1}{S_{wc}} \tag{14}$$

$$R_c = \frac{e_c}{k_c \cdot S_c} \tag{15}$$

Where k_{it}, k_g, k_c are thermal conductivities of inter-turns material, gap in the window and core material respectively. S_{it}, S_{wc} and S_c are sections of various elements.

3.2.4. R_{ex}: This thermal resistance (Fig.8b) represents the heat exchange with the environment (16).

$$R_{ex} = \frac{1}{h_{ex} \cdot S_{ex}} \tag{16}$$

Where h_{ex} is the global heat exchange coefficient of the area (S_{ex}) to the exterior, Calculation of this coefficient is detailed in section 3.5.

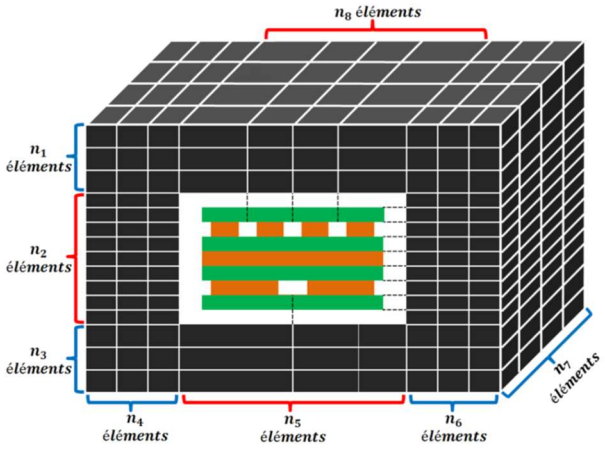

a

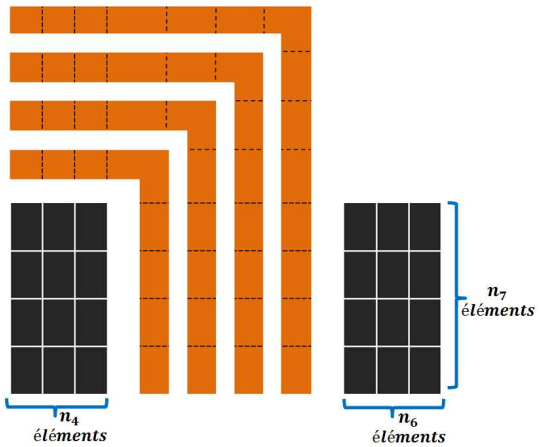

b

Fig. 6. *Discretization*
(a) Magnetic core, ***(b)*** Windings

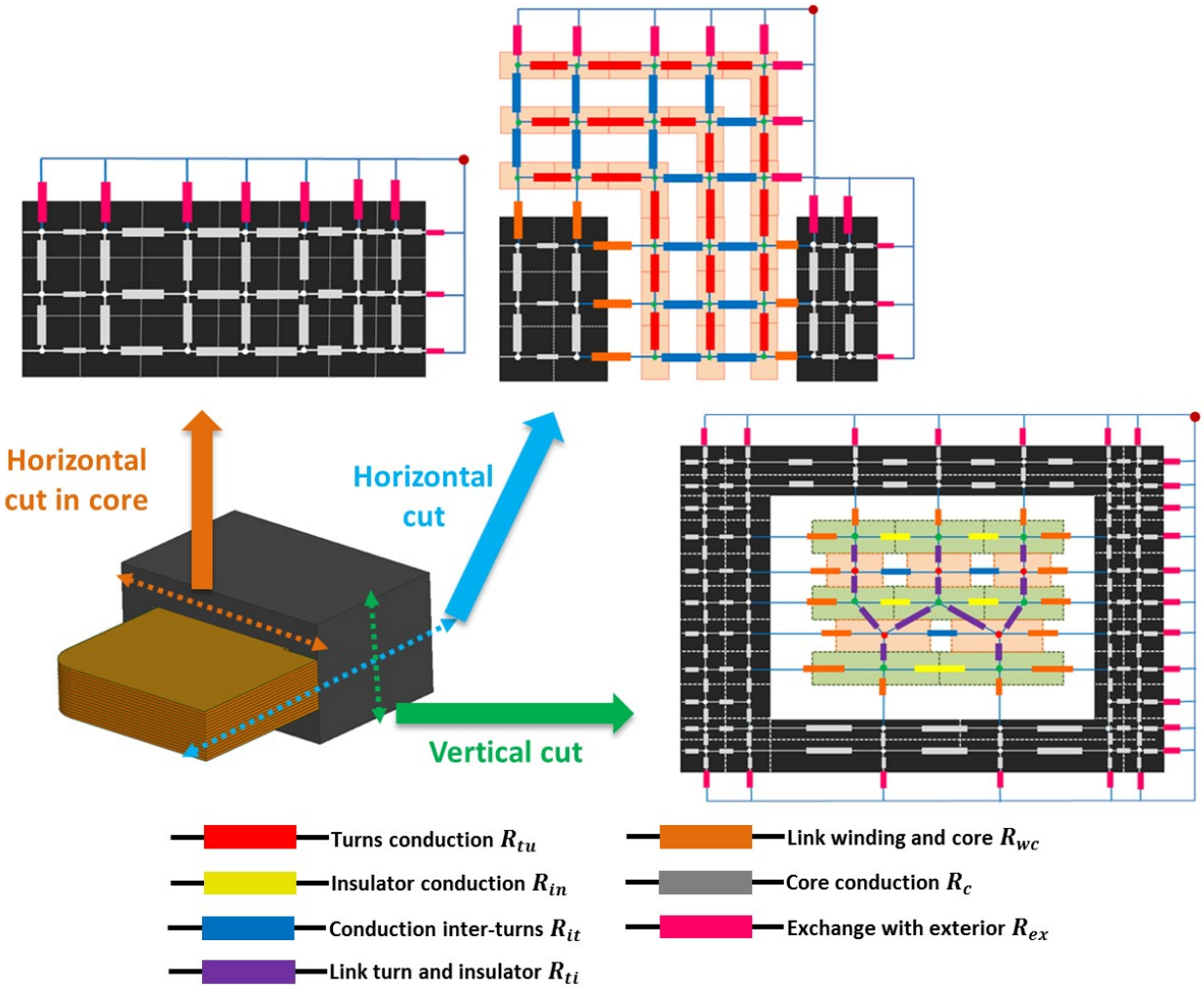

Fig. 7. *Global discretization with thermal resistances*

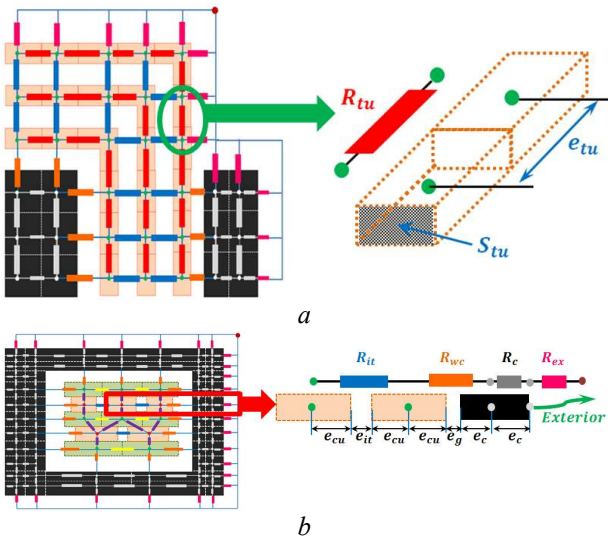

Fig. 8. *Elementary thermal resistances*
(a) R_{th} between two adjacent elements of a turn ***(b)*** R_{th} for inter-turns, winding-core, core and heat exchange with environment

3.2.5. R_{ti}: It models the conduction phenomena between a node from a copper turn and another one from insulator (Fig.9). The intersection area S_i is taken into account in the calculation of the thermal resistance value (17).

$$R_{ti} = \left(\frac{e_1}{k_{Cu}} + \frac{e_2}{k_i} \right) \cdot \frac{1}{S_i} \qquad (17)$$

3.3. Thermal capacitances

In order to solve transient cases, dynamic effects must be integrated in the thermal modelling. Capacitances are then added between each node of the planar magnetic component. The thermal capacitance of an elementary volume is given by (18).

$$C_i = c_m . \rho . V_i \qquad (18)$$

Where V_i is the volume of material, c_m the heat capacity and ρ the density.

3.4. Power losses

Power losses are a main input parameter of TATPM. They can be evaluated with any type of model. For copper losses, 1D analytical models [26] can only give global losses. Therefore, for such model, all the conductors would have the same amount of losses. In order to obtain separated values for any single conductor, 2D or 3D models [27, 28] are required.

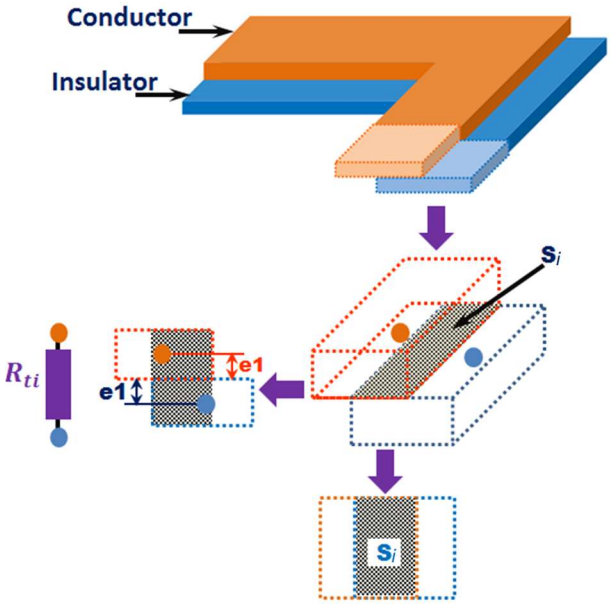

Fig. 9. *Thermal resistance linking conductor to insulator*

Copper losses and core losses need to be distributed inside the component. As a consequence, losses are changed to volumetric ones by dividing each kind of losses by the volume of copper turns and magnetic core respectively. Then, for every discretization element, the amount of losses q_i (19) is obtained with the product of the element volume V_i and the volumetric losses p_v.

$$q_i = p_v.V_i \tag{19}$$

The layout of TATPM also allows a magneto-thermal coupling. Based on the automatic geometrical description, loss computation could be performed directly using adequate model. The obtained values would be used as input of TATPM.

Moreover, copper and core losses can also depend on temperature. In this case, it is possible to couple TATPM with temperature dependent losses models. Another alternative consists in evaluating losses at a guessed operating temperature of the component, which is a faster method to take into account the effect of temperature on losses.

3.5. Boundary conditions

Heat transfer between the component and its environment (exterior) needs to be specified under the form of boundary conditions (BC). The latter are applied to the external area of the component's winding and core (Fig.10) to take into account convection and radiation effects. Three types of BC can be applied to the various external surfaces:

i. Top or/and bottom of core with fixed temperature (faces S4 and S5 shown in Fig.10)
ii. Constant heat coefficients on external areas
iii. Temperature dependent heat coefficients on external areas

The last case is typical for natural convection where the convection coefficient depends on the geometry of the surface, its orientation and its temperature evolution.

Convection coefficients that can be applied to the component's external faces [29] are listed in equation (20), (21) and (22). They correspond to 3 cases: horizontal plate top heating with a width W (Fig.11a) or bottom heating with a width W (Fig.11b) and vertical plate with height H (Fig.11c), respectively.

$$h_c = 1.32 \cdot \left(\frac{\Delta T}{W}\right)^{0.25} \tag{20}$$

$$h_c = 0.66 \cdot \left(\frac{\Delta T}{W}\right)^{0.25} \tag{21}$$

$$h_c = 1.42 \cdot \left(\frac{\Delta T}{H}\right)^{0.25} \tag{22}$$

Radiation effect has to be added to the convection one. Equivalent radiation transfer coefficients can be derived from Stefan Boltzmann law given by (23). Then, global coefficients applied to the component external faces are the sum of the resulting coefficients calculated from the two heat transfer modes (24).

$$h_r = \sigma \cdot \varepsilon \cdot \frac{T_s^4 - T_a^4}{T_s - T_a} \cdot \tag{23}$$

With:
σ: Stephan Boltzmann constant 5.6710^{-8} W m^{-2} K^{-4}
ε: Surface emissivity
T_a: ambient temperature in K
T_s: surface temperature in K

$$h_{ex} = h_c + h_r \tag{24}$$

3.6. Solving process

The TATPM offers four types of problem solving, in transient or steady state, with constant or temperature dependent BC (Fig.3).

3.6.1. Steady state/Constant temperature BC: Based on the data inputs described above, thermal resistances are calculated as explained in section 3.2. Then, with these elements, matrixes A, B, and U (6) are computed in order to solve equation (8). Finaly, the temperature vector T is obtained in the case of a steady state study, with constant heat exchange coefficient.

3.6.2. Steady State/Temperature dependent BC: In the case of temperature dependent heat exchange coefficients, a convergence criterion is added. If these criterions are not verified, the BC are re-evaluated from the mean temperatures of the different external surfaces of the component. Then, thermal resistances representing the heat exchange with the environment are computed again to obtain new matrixes A and B. Finally, the temperature vector is also recomputed. This process is repeated until convergence. The convergence is reached if, between two successive iterations, the norm of the computed temperature vectors difference is lower than the stopping criteria.

3.6.3. Transient/Constant temperature BC: In transient analysis with constant heat exchange coefficients, temperature vector is computed with the equation (10) for each iteration until completing the simulation time specified by the user.

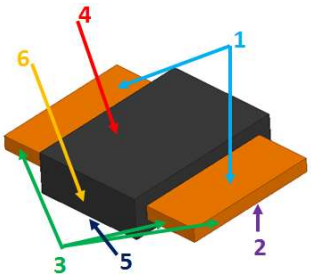

Surface	Description
S1	Top-winding
S2	Down-winding
S3	Lateral-winding
S4	Top-core
S5	Down-core
S6	Lateral-core

Fig. 10. *External area boundary conditions*

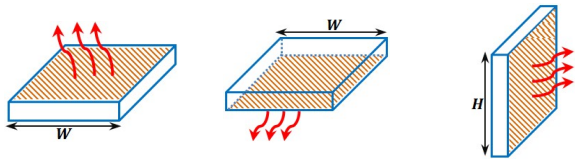

Fig. 11. *Natural convection heat transfer for plate*
(a) Horizontal plate top heating with a width W (20), **(b)** Horizontal plate bottom heating with a width W (21), **(c)** Vertical plate with height H (22)

3.6.4. Steady State/Temperature dependent BC: In the case of transient analysis with temperature dependent heat exchange coefficients, the computation is completed in two-steps evaluation: The first step is a steady state computation with temperature dependent heat exchange coefficients (section 3.6.2). In a second step, these exchange coefficients are used to perform the transient problem solving with constant heat exchange coefficients (section 3.6.3).

4. Validation and discussion

In order to validate and to explore all capacities of TATPM, two planar transformers are designed and tested with different study conditions. For each planar transformer, results from TATPM are first compared to thermal FEM ones. Then, results from TATPM are compared to thermal measurements on prototypes. The section ends with discussion on the results and the benefits of using TATPM.

4.1. Studied Cases

The two transformers are described in Fig.12a. Study conditions that are stated on fig.12b are used for the FEM simulations. Other conditions are taken into account to validate the comparison with experimental results.

The first transformer (Tr1) is designed for a power of 360 VA. Windings are made of 12 copper layers separated by Kapton layers as insulator. The 6 first layers form the 3-turns of primary winding (two parallel layers by turn) while the 6 other layers are all parallelized to form the secondary winding. The second transformer (Tr2) is designed for a 2kVA power. Primary winding is made of 4 copper layers connected in series, with 4 turns by layer to form 16 primary turns. Secondary winding is made of 4 layers connected in parallel to form the secondary. Primary and secondary layers are alternated as shown in Fig.13. The two transformers are made with 3F3 E/PLT38 and 3F3 E/PLT58, respectively. Core dimensions and 3F3 ferrite properties could be found in [25]. Electrical specifications of both transformers are listed in Table 1.

Regarding losses, copper and core losses are estimated under sinusoidal excitations, with currents and voltages specified in Table 1. Copper losses in each conductor are computed with 2D FEA using FEMM software [30]. Core losses (25) are computed using Steinmetz formula [31]. Losses of each transformer appear in Table 1.

$$P_{core} = k_{st} \cdot f^{\alpha} \cdot B_{max}^{\beta} \cdot V_{core} \qquad (25)$$

Where B_{max} is the maximum flux density, V_{core} is core volume, k_{st} , α and β are coefficients given by core manufacturers. These coefficients depend on the ferrite material, the temperature and the frequency range [14]. For both studies, 3F3 ferrite is used with k_{st}=0.25E-3, α=1.63 and β=2.45 at 100 °C.

4.2. Comparison with FEM simulation results

In this section, both transformer Tr1 and Tr2 are modelled using TATPM and FEM. Results are compared in terms of temperature inside magnetic core and windings.

FEM is an accurate solution for modeling the heat transfer mechanisms: conduction, convection and radiation. FEM is frequently used to study the thermal behavior of magnetic components [10, 24, 32, 33]. It solves the same problem as TATPM which is heat equation associated with convection and radiation represented by heat exchange coefficients.

CFD also could be performed but the size of the computational problem and the nonlinearities of the solved equations lead to necessary strong geometry simplifications. For example, in the case of planar magnetics, the required homogenization of windings results in a loss of details on temperature distribution. Finally, with CFD, only a global thermal modeling would be achieved such as in [18].

Table 2 presents thermal properties of materials used in planar transformers [29]. These values are implemented in TATPM and Ansys software [34] for the FEM simulations.

The ambient temperature is set to 30°C for both cases. Regarding boundary conditions (Fig.12b), the transformer Tr1 is free air cooled. Temperature dependent heat exchange coefficients are used to model the free convection and radiation, as detailed in part 3.6.2. Losses inside transformer Tr2 lead to high temperatures with free air cooling. Then, the temperature on the bottom side of the magnetic core is fixed to 80°C representing the cooling system effect (Fig.12b).

Table 1 Planar transformer electrical and geometrical properties

	Transformer (Tr1)	Transformer (Tr2)
Power rating [VA]	360	2000
Input voltage [V]	40	400
Input current [A]	9	5
Working frequency [kHz]	100	100
Output voltage [V]	13	25
Copper thickness [mm]	0.2	0.35
Insulator thickness [mm]	0.12	0.07
Winding mean length [mm]	130	180
Magnetic core	E/PLT 38	E/PLT 58
Copper losses (W)	3	4.21
Core losses (W)	3.07	12.49

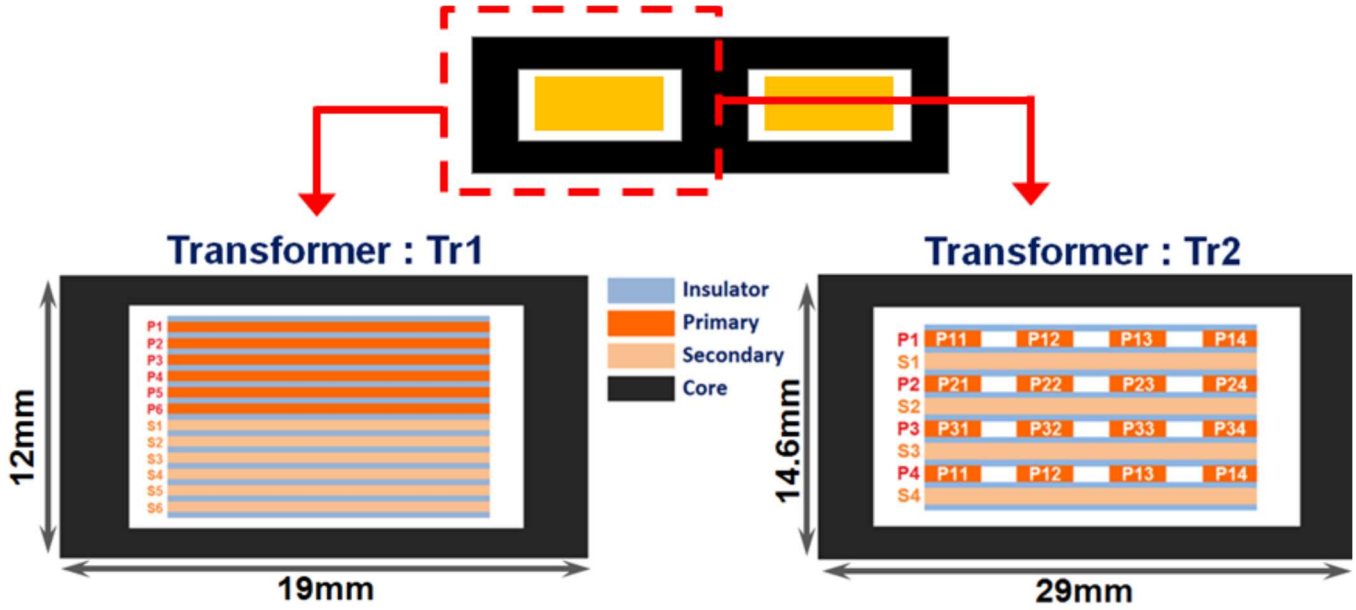

a

b

Fig. 12. *Planar transformers Tr1 and Tr2:*
(a) Winding configurations **(b)** condition studies for the comparison of TATPM and FEM results

Table 2 Material properties

Material	Thermal conductivity [W m^{-2} K^{-1}]	Massic heat capacity [J kg^{-1} K^{-1}]	Emissivity
Copper	380	480	
Ferrite	4	700	0.9
Insulator (Kapton)	0.15	1100	0.45
Air	0.025	1200	

Final temperature distributions computed by TATPM and by FEM are shown in Fig.13 and Fig.14 for Tr1 and Tr2, respectively. In the subfigures a and b, the overall temperature distribution on the component enables to compare results of winding and magnetic core. In the subfigures c and d, the results are only focused on temperature distribution inside windings for both components. Temperature distributions computed with TATPM and FEM show a good agreement. In order to compare temperatures obtained with both models, table 3 lists minimum and maximum temperature values in windings and core for Tr1 and Tr2. Error between both models does not exceed 8.4°C. TATPM tends to overestimates temperature in comparison with FEM, except for Tr1 winding's temperature.

The maximal temperature obtained with TATPM for transformer Tr1 could be compared to the one obtained with one equivalent thermal resistance. Based, on [15], the thermal resistance of the component can be estimated (26). Temperature can be calculated with (27). This value is consistent with the ones obtained in the magnetic core with TATPM and FEM (Table 3).

$$R_{th} = \frac{1000}{24 \cdot V_e^{0.54}} = \frac{1000}{24 \cdot 8.46^{0.54}} = 13.15°C/W \quad (26)$$

with V_e the effective volume of the core in [cm^3]

$$T_{max} = R_{th} \times P + T_a = 13.15 \times 6.07 + 30 = 109.8°C \quad (27)$$

Then, transformer Tr2 is studied in transient analysis. The same losses is applied while the boundary conditions are taken from the steady state case. Fig.15a compares the temperature evolution obtained with TATPM and FEM. The two curves are very close. Time constants for both responses are 1000s and 960s for TATPM and FEM, respectively. The error between TATPM and FEM is shown in Fig.15b. This error remains under 9°C on the time interval.

Using TATPM, the steady state case for Tr1 was solved in 5 seconds. The exchange coefficients on the external surface were changed according to the temperature. Their final values were obtained for the 6th iteration. The geometry (Fig.2) of the Tr1 planar transformer was divided in 1889 discretised elements. For transformer Tr2, the transient analysis was solved in 5.32 minutes. Its geometry was divided in 2587 elements.

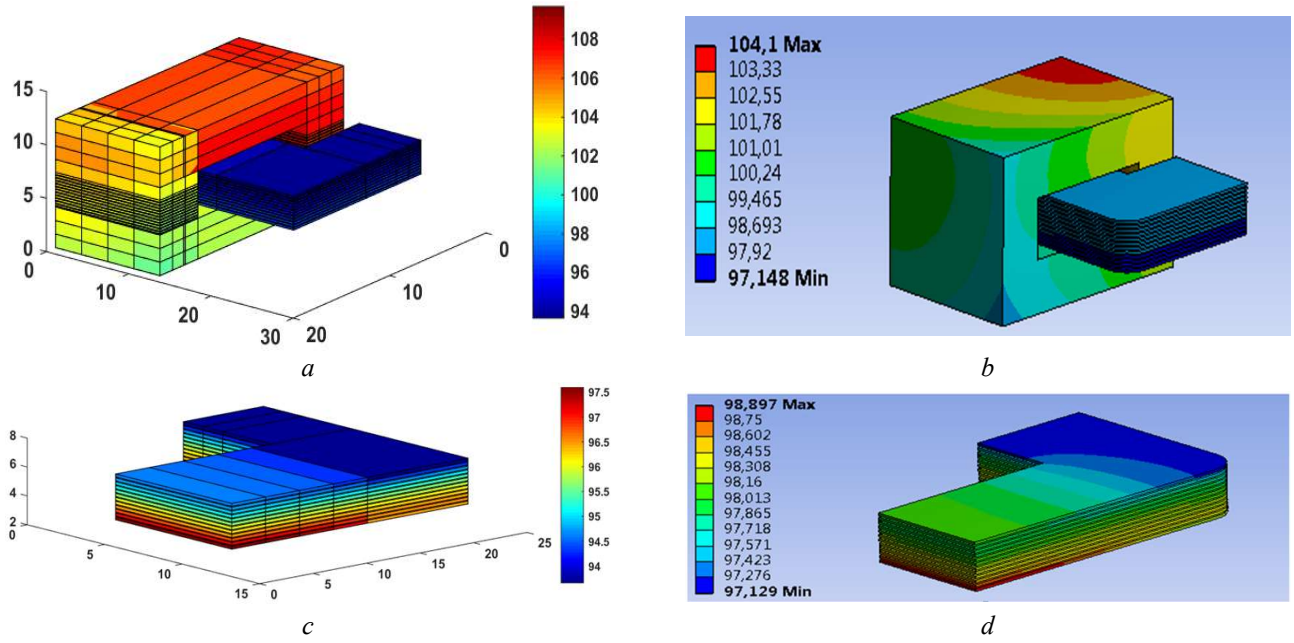

a *b* *c* *d*

Fig. 13. *Temperature distribution for Tr1*
(a) Tr1 with TATPM, **(b)** Tr1 with FEM, **(c)** Tr1 winding with TATPM, **(d)** Tr1 winding with FEM

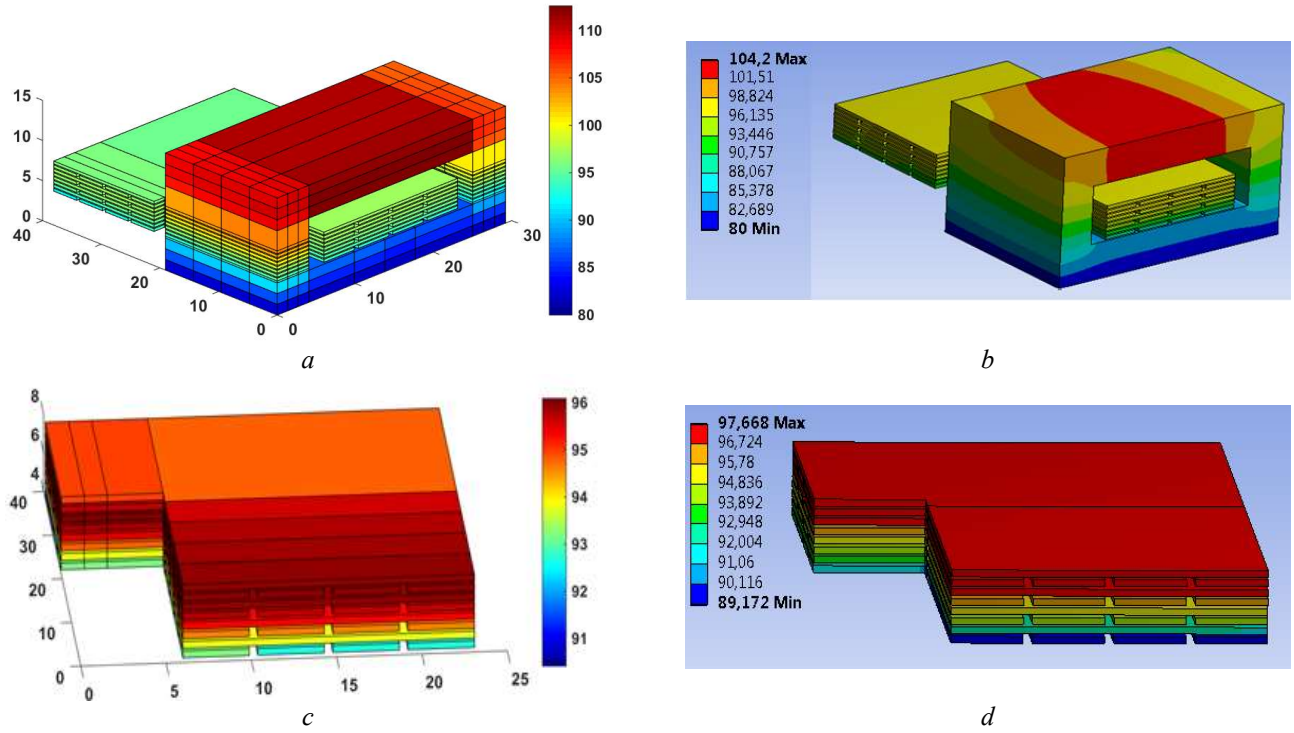

a *b* *c* *d*

Fig. 14. *Temperature distribution for Tr2*
(a) Tr2 with TATPM, **(b)** Tr2 with FEM, **(c)** Tr2 winding with TATPM, **(d)** Tr2 winding with FEM

4.3. Experimental validation

Two transformers have been developed based on the design introduced in the previous section. Fig.16 shows the two planar transformer prototypes.

The best way to valid a transformer design is to test prototypes in their application/converter with their nominal power. In this case, measurement of losses is quite complex. Indeed, measuring 20W losses with 1W precision, while total power is close to 2kW, needs equipment with a precision under 0.05%. Then, precise measurements are quite difficult to achieve [35].

To circumvent this problem, in order to compare TATPM with measurement results, loss values are imposed with open circuit and short-circuit test configurations. For Tr1, a secondary open circuit test enables to set losses in transformer by acting on the supply voltage value. In that case, main losses are core ones. For Tr2, a secondary short-circuit test is preferred. With such test, main losses are copper ones. Then, current and losses are adjusted by acting on the primary supply voltage. However, this method is only suitable for planar transformer with good thermal coupling between windings and magnetic core. Indeed, heat must be distributed

throughout the component in order to ensure actual representation of thermal heating.

A HF full bridge [36] has been developed to perform these tests. The bridge is made of STP36N55M5 MOSFET [37] with ADUM3223BRZ gate drivers [38]. The open loop phase-shift command is achieved with DSP TMS320F28335 [39]. Oscilloscope (Tektronix DPO 4034 [40]) measurements are made with LEM PR50 current probe [41] and ST1000-II voltage probe [42]. Prototypes' temperatures are measured with a thermal camera Fluke TI95 [43].

Tr1 is supplied with open-circuit secondary. Losses are set to 6W. Tr2 is supplied with short-circuit secondary. Losses are set to 15W. Both transformers are tested in free air (i.e natural convection) in an ambient temperature of about 30°C. These test conditions are different from the studied conditions of part 4.2, so TATPM was relaunched under these new losses and temperature measurement conditions.

The Table 4 shows temperatures measured in the different parts of each prototype. Measured values show a good agreement with computed ones. Indeed, the temperature absolute error does not exceed 8.8°C. For prototype Tr1, magnetic core has a higher temperature than for the windings because of losses that are located inside the core. On the opposite, for prototype Tr2, windings have higher temperature than the core due to copper losses in primary and secondary.

Thus, TATPM computes 3D-temperature distribution with satisfactory accuracy, even if temperature are slightly overestimated. This overestimation can be used as a safety margin in the design process.

4.4. Discussion

TATPM has been validated with FEM simulations and experimental measurements. Two different transformers have been designed and tested with various operating conditions, in order to show the capacities of TATPM.

TATPM presents a rather good accuracy/computation time ratio: The obtained accuracy remains good with low computation time. These both criteria depend on the number of discretized elements. Compared to FEM simulations, TATPM has less elements. The computation is faster, but computation results are less precise.

Due to its performances and its automatic geometry and lumped element computation, the presented TATPM can be used during the design process to study the thermal integrity of planar magnetic components, or for investigating the cooling requirement and the cooling system effect on thermal performances. TATPM enables to perform fast design checking for all EE and E/PLT core based planar transformers and inductors. The solving process is selectable by the user: steady state and transient case with or without temperature dependent coefficients. These options enable multiple case studies for planar components.

Finally, TATPM could also be coupled with magnetic modelling to perform magneto-thermal computations and optimization tools to achieve an overall components' optimization.

5. Conclusion

In this paper, a thermal automated tool for planar magnetics has been developed. The thermal model is based on thermal resistance networks. Modelling principle and its implementation are detailed. The obtained temperature distribution in windings and magnetic core is represented in 3D.

Table 3 Temperature comparison TATPM/FEM

	TATPM (°C)	FEM (°C)	Error (°C)	Error (%)
Tr1 – windings – Min	93.66	97.13	-3.47	-3.7
Tr1 – windings – Max	97.61	98.9	-1.29	-1.3
Tr1 – magnetic core – Min	101.15	98.18	2.97	2.9
Tr1 – magnetic core – Max	109.69	104.13	5.56	5
Tr2 – windings – Min	91.15	89.03	2.12	2.3
Tr2 – windings – Max	98.01	97.45	0.56	5.7
Tr2 – magnetic core – Min	80	80	0	0
Tr2 – magnetic core – Max	112.59	104.20	8.39	7

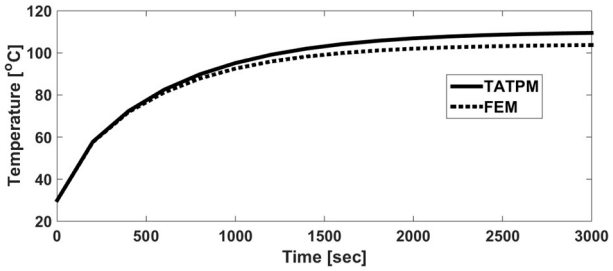

a

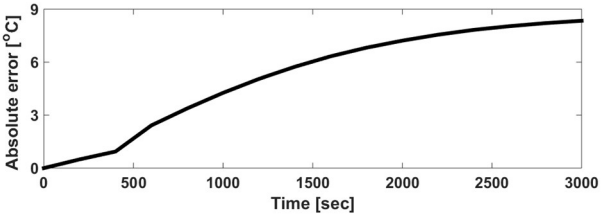

b

Fig. 15. *Transient case for Tr2*
(a) Maximal temperature evolution with time for the TATPM and FEM, **(b)** Absolute error between TATPM end FEM results

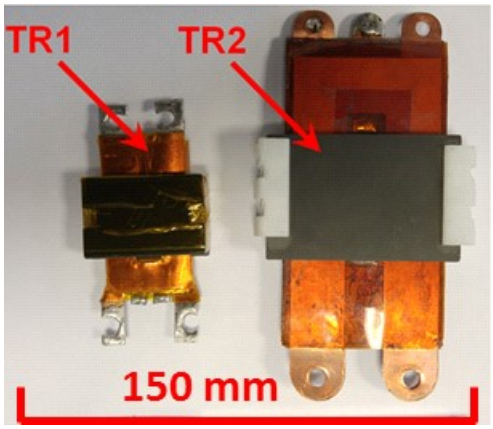

Fig. 16. *Planar transformers prototypes*

Table 4 Temperature comparison TATPM/Experimental

	Model (°C)	Measurement (°C)	Error (°C)	Error (%)
Tr1 – windings	96.54	95.6	-0.94	<1
Tr1 – magnetic core	110.98	102.2	-8.78	7.9
Tr2 – windings	131.13	125	-6.13	4.6
Tr2 – magnetic core	102.40	98	-4.4	4.2

It presents a good agreement with temperature distributions computed by FEM. TATPM has been validated through experimental measurements on two prototypes with a very good accuracy.

One of the main advantages of our model and its associated tool deals with the lumped elements automatic computation according to the component's geometry. Thus each type of EE and E/PLT core based planar transformers or inductors can be easily modelled with a good precision. The use of TATPM can facilitate design tasks, cooling studies or components' optimization.

Such model could also be used in real time simulation for the virtual prototyping of planar magnetics for power converters. Hardware-in-the-loop (HIL) and dynamic loss model can be combined with TATPM to estimate the real thermal behavior of a studied component in a conception phase.

6. References

[1] Kolar, J. W. *et al.*: 'PWM Converter Power Density Barriers'. Proc. 2007 Power Conversion Conference – Nagoya, Japan, pp. 9-29

[2] Biela, J., Badstuebner, U., Kolar, J. W.: 'Impact of Power Density Maximization on Efficiency of DC–DC Converter Systems', *IEEE Transactions on Power Electronics*, 2009, **24**, (1), pp. 288-300

[3] van Wyk, J. D., Lee, F. C.: ' On a Future for Power Electronics ', *IEEE Journal of Emerging and Selected Topics in Power Electronics,* 2013*,* **1**, (2), pp. 59-72

[4] Guan, Y., Wang, Y., Xu, D., Wang, W.: 'A 1 MHz Half-Bridge Resonant DC/DC Converter Based on GaN FETs and Planar Magnetics', *IEEE Transactions on Power Electronics*, 2017, **32**, (4), pp. 2876-2891

[5] Zhang, Z., Ngo, K. D. T.: 'Multi-megahertz quasi-square-wave flyback converter using eGaN FETs', *IET Power Electronics*, 2017, **10**, (10), pp. 1138-1146

[6] Ouyang, Z., Andersen, M. A. E.: ' Overview of Planar Magnetic Technology—Fundamental Properties', *IEEE Transactions on Power Electronics*, 2014, **29**, (9), pp. 4888-4900

[7] Ngoua Teu Magambo, J. S. *et al*: ' Planar Magnetic Components in More Electric Aircraft: Review of Technology and Key Parameters for DC–DC Power Electronic Converter', *IEEE Transactions on Transportation Electrification*, 2017, **3**, (4), pp. 831-842

[8] Saket, M. A., Shafiei, N., Ordonez, M.: ' LLC Converters With Planar Transformers: Issues and Mitigation', *IEEE Transactions on Power Electronics*, 2017, **32**, (6), pp. 4524-4542

[9] Boglietti, A., Cavagnino, A., Staton, D., Shanel, M., Mueller, M., Mejuto, C.: 'Evolution and Modern Approaches for Thermal Analysis of Electrical Machines', *IEEE Transactions on Industrial Electronics*, 2009, **56**, (3), pp. 871-882

[10] Puigdellivol, O., Méresse, D., Menach, Y. L., Harmand, S., Wecxsteen, J.: 'Thermal Topology Optimization of a Three-Layer Laminated Busbar for Power Converters', *IEEE Transactions on Power Electronics*, 2017, **32**, (6), pp. 4691-4699

[11] McLyman, C.W. T.: 'Transformer and inductor design handbook' (4. ed. Boca Raton, Fla. CRC Press, 2011)

[12] van den Bossche, A., Valchev: 'Inductors and transformers for power electronics ' (Boca Raton: Taylor and Francis, 2005)

[13] Tria, L. A. R., Alam, K. S., Zhang, D., Fletcher, J. E.: 'Comparative study of multicore planar transformers on printed circuit boards', *IET Power Electronics*, 2017, **10**, (12), pp. 1452-1460

[14] 'Design of Planar Power Transformers', 2000, http://ferroxcube.home.pl/appl/info/plandesi.pdf, accessed 11 october 2018

[15] Ferroxcube Soft Ferrites Design Tool (SFDT), april 2010, https://www.ferroxcube.com/en-global/design_tool/index, accessed august 9 2019

[16] Muldoon, W. J.:' Analytical design optimization of electronic power transformers', *Proc.* IEEE Power Electronics Specialists Conference, Syracuse, NY, 1978, pp. 216-225

[17] 'Magnetics Designer - Personal Computer Circuit Design Tools', 2013, http://www.intusoft.com/lit/Magdes.pdf, accessed 11 october 2018

[18] Bakri, R., Teu, J. S. N., Margueron, X., Le Moigne, P., Idir, N.: ' Planar transformer equivalent thermal resistance variation with ambient temperature and power losses', Proc. *2016 18th European Conference on Power Electronics and Applications (EPE'16 ECCE Europe)*, Karlsruhe, Germany, pp. 1-9

[19] Smit, M. C., Ferreira, J. A., van Wyk, J. D., Ehsani, M.: 'Technology for manufacture of integrated planar LC structures for power electronic applications ', Proc. *1993 Fifth European Conference on Power Electronics and Applications*, Brighton, UK, 2, pp. 173-178

[20] Lewaiter, A., Ackermann, B.: 'A thermal model for planar transformers', *Proc.* 4th IEEE International Conference on Power Electronics and Drive Systems. IEEE PEDS, Denpasar, Indonesia, 2001, 2, pp. 669-673

[21] Buccella, C., Cecati, C., de Monte, F.: 'A Coupled Electrothermal Model for Planar Transformer Temperature Distribution Computation', *IEEE Transactions on Industrial Electronics*, 2008, 55, (10), pp. 3583-3590

[22] Buccella, C., Cecati, C., de Monte, F.: 'A computational method of temperature distribution in high frequency planar transformers', 2011 IEEE International Symposium on Industrial Electronics, Gdansk, 2011, pp. 477-482

[23] Bernardoni, M., Delmonte, N., Cova, P., Menozzi, R.: 'Thermal modeling of planar transformer for switching power converters', *Microelectronics Reliability*, 2010, 50, (9), pp. 1778-1782

[24] Shafaei, R., Ordonez, M., Saket, A.: 'Three-Dimensional Frequency-Dependent Thermal Model for Planar Transformers in LLC Resonant Converters', *IEEE Transactions on Power Electronics*, 2019, 34, (5) pp. 4641-4655

[25] 'Soft Ferrites and Accessories Data Handbook 2013', https://www.ferroxcube.com/en-global/download/download/11, accessed 11 october 2018

[26] Dowell, P. L.: 'Effects of eddy currents in transformer windings', *Proceedings of the Institution of Electrical Engineers*, 1966, 113, (8), pp. 1387–1394

[27] Robert, F., Mathys, P., Schauwers, J., 'Ohmic losses calculation in SMPS transformers: numerical study of Dowell's approach accuracy', *IEEE Transactions on Magnetics*, 1998, 34, (4), pp. 1255-1257

[28] Taylor, L., Margueron, X., Le Menach, Y., Le Moigne, P.: 'Numerical modelling of PCB planar inductors: impact of 3D modelling on high-frequency copper loss evaluation', *IET Power Electronics*, 2017, 10, (14), pp. 1966-1974

[29] Incropera, F.: 'Fundamentals of Heat and Mass Transfer' (New York: John Wiley and Sons, 1985)

[30] Meeker , D., D.: 'Finite Element Method Magnetics', http://www.femm.info/wiki/HomePage/, accessed 11 october 2018

[31] Brittain, J. E.: 'A steinmetz contribution to the AC power revolution', *Proc. IEEE*, 1984, 72, (2), pp. 196–197

[32] Salinas G., Delgado A., Oliver J. A., Prieto R.: 'Fast FEA Thermal Simulation of Magnetic Components by Winding Equivalent Layers', Proc. *2018 IEEE Energy Conversion Congress and Exposition (ECCE)*, Portland, OR, 2018, pp. 7380-7385.

[33] Shafaei R., Saket M. A. and Ordonez M.: Thermal 'Comparison of Planar Versus Conventional Transformers Used in LLC Resonant Converters', Proc. *2018 IEEE Energy Conversion Congress and Exposition (ECCE)*, Portland, OR, 2018, pp. 5081-5086.

[34] 'ANSYS - Simulation Driven Product Development', http://www.ansys.com, accessed 11 october 2018

[35] Keradec, J.: 'Validating the power loss model of a transformer by measurement - Validation is key', *IEEE Industry Applications Magazine*, 2007, 13, (4), pp. 42-48

[36] Mutlu, U.: 'Analysis, Design, And Implementation Of A 5 Kw Zero Voltage Switching Phase-Shifted Full-Bridge Dc/Dc Converter Based Power Supply For Arc Welding Machines', Master thesis, Middle East Technical University, 2006.

[37] STP36N55M5 Power MOSFET datasheet, Doc ID 022902 Rev 2 October 2012, http://www.st.com, accessed august 9 2019

[38] ADUM3223BRZ Isolated Precision Half-Bridge Driver datasheet, Rev. J, http://www.analog.com, accessed august 9 2019

[39] TMS320F2833x, TMS320F2823x Digital Signal Controllers (DSCs), SPRS439O –June 2007–Revised april 2019, http://www.ti.com, accessed august 9 2019.

[40] Tektronix 4000 Series Digital Phosphor Oscilloscopes User Manual, 071-2121-00, http://www.tektronix.com, accessed august 9 2019

[41] PR 50 Universal 50 MHz Current Probe for Oscilloscopes, Publication GB20601 E, http://www.lem.com, accessed august 9 2019

[42] Differential Voltage Probe ST 1000-II, https://www.francaise-instrumentation.fr/sondes-differentielles/50-sonde-differentielle-30-mhz-2-voies.html, accessed august 9 2019

[43] 'Ti90, Ti95 Ti100, Ti105, Ti110, Ti125 TiR105, TiR110, TiR125 Performance Series Thermal Imagers Users Manual', https://www.myflukestore.com, accessed 11 october 2018